The Pennsylvania State University

The Graduate School

Department of Chemical Engineering

COARSENING DYNAMICS OF BINARY LIQUIDS UNDER ACTIVE ROTATION

A Thesis in

Chemical Engineering

by

Syeda Sabrina

Submitted in Partial Fulfillment
of the Requirements
for the Degree of

Master of Science

December 2014

The thesis of Syeda Sabrina was reviewed and approved* by the following:

Kyle J. M. Bishop
Assistant Professor of Chemical Engineering
Thesis Advisor

Darrell Velegol
Distinguished Professor of Chemical Engineering

Scott T. Milner
Joyce Chair
Professor of Chemical Engineering

Themis Matsoukas
Professor of Chemical Engineering

Michael Janik
Graduate Program Coordinator
Associate Professor of Chemical Engineering
John J. and Jean M. Brennan Clean Energy Early Career Professor in
College of Engineering

*Signatures are on file in the Graduate School

ABSTRACT

Active matter comprised of many self-driven units (*e.g.* colloidal swimmers) exhibits emergent collective behaviors such as clustering, swarming and segregating depending on the nature of the local energy input, the nature of the energy dissipation, and the interactions between the individual units. In a recent microscopic model of actively rotating spinners[1], it was shown that a binary mixture of particles under active rotation phase separate into domains of like-rotating particles in 2-dimensions (2D). The size of these domains R, grows in time as $R \sim t^{1/3}$ under "weak" rotation with frictional drag as the dominant damping force. This result is in agreement with the classic diffusion-controlled demixing of passive binary liquid mixtures without active rotation. Other more exotic types of coarsening are anticipated in this nonequilibrium system as a function of the strength of active rotation as compared to that of frictional damping and viscous damping in the system. Here we develop a continuum 2D model of phase separation in binary liquids under active rotation and systematically explore its different dynamical regimes. Our model combines the convective Cahn-Hilliard equation governing the local composition field and the Navier-Stokes equation with active rotation and frictional damping governing the velocity field. Besides recovering diffusion-controlled coarsening under conditions of "weak" rotation, our model predicts a variety of new behaviors such as active coarsening and the emergence of "vortex-doublets".

These numerical results are reproduced and explained by scaling arguments that outline the different dynamical regimes and elucidate the diverse behaviors therein.

TABLE OF CONTENTS

LIST OF FIGURES

Chapter 1

Introduction

There has been a growing interest in the study of collective behaviors of nonequilibrium systems comprising many self-driven particles[2–4]. Examples span many length scales, with the most preeminent ones found in living systems, ranging from subcellular to oceanic. Living systems such as bacterial suspensions, bird flocks, and fish schools exhibit fascinating collective motion. The common feature of these diverse groups in nature is that non-equilibrium interactions among the constituents give rise to dynamic organization and emergent structures qualitatively different from the individual units. Besides their biological importance, these systems offer opportunities to harness useful mechanical work from their collective motions as well as inspiration in design of biomimetic machines[5–7] and smart materials[8]. Such ensembles of active "particles" exhibit unique nonequilibrium features such as autonomous motility that are strikingly different from materials assembled from passive building blocks. Unlike equilibrium systems, there are no general principles that govern the dynamics of these nonequilibrium ensembles. It is necessary to develop our fundamental understanding of these systems in order to engineer their collective behaviors towards performing useful functions.

1.1 Motivation

Active materials are nonequilibrium systems comprising many self-driven units that consume and dissipate energy individually[2]. Unlike classic nonequilibrium systems (*e.g.*, a fluid under shear), the energy input in active matter is provided at the scale of the individual units. Despite the simple motions of their individual units, active matter exhibits complex collective motions that emerge from the interactions among units themselves.

In nature collective behaviors such as swarming[9], clustering[10], and pattern formation[11] have been observed over many length scales, ranging from suspensions of motile microorganisms[12] to animal groups[4]. Such collective motions can be harnessed in mechanical systems to extract useful energy. Examples include micro-gear wheels powered by bacterial motions[13,14]. Suspensions of microswimmers also exhibit tunable properties such as reduced viscosity[15] and increased diffusivity[16]. Ensembles of non-living or synthetic active particles such as catalytic swimmers[17], vibrated granular rods[18], and self-propelled droplets[19] may also achieve these properties without any biological components. It should therefore be possible to mimic the collective behaviors of living systems in artificial materials to engineer smart materials and systems capable of complex actuation, self-healing, autonomous motion and shape change.

1.2 Background

One of the main challenges in development of bio-inspired machines and materials is that very little is understood about the fundamental principles of underlying collective motions. Vicsek *et al* did the pioneering work in study of collective motion of active matter[20]. Since then very few studies have investigated collective behaviors due to active rotation[1,21–24], whereby the local energy input is converted into rotational motion of the constituent units. Active rotation has been observed in biological systems such as swimming algae[25] and bacterial carpet[26] and also in artificial systems such as actively rotating disks and chiral spinners at air-liquid interface [21,24]. In a recent study the Glotzer group has systematically explored the emergent collective dynamics of many rotationally driven disks, called spinners[1] in 2D. Each spinner was modeled as hard particle driven by an external torque of constant magnitude such that half of them rotate in clockwise direction and the rest rotate in counterclockwise direction. They characterized the phase behavior of the spinners as a function of their angular velocity and density. At sufficiently high density the spinners phase separate and form domains of like-rotating particles. As the density is increased further they organize into rotating crystals. Such activity induced phase transitions have also been observed in other active systems both experimentally[27–29] and computationally[30–32]. Remarkably, the domain size (R) of the spinners grows in time as $R \sim t^{1/3}$ which is typically observed in diffusion-controlled phase separation of binary mixture without any active driving force. These simulation studies were limited to the overdamped regime, in which active rotation was weak relative to frictional drag. We anticipate that other more exotic phase behaviors may be

observed for different strengths of active rotation, frictional damping, and viscous damping in the system. Here, we develop a phenomenological, continuum model of phase separation in a system under active rotation and investigate its dynamics under a variety of different conditions.

1.3 Thesis Outline

Chapter 2 presents the theoretical background on coarsening dynamics of passive binary liquids. Here the term passive implies that there is no active rotation in the system. Then we extend these theories to account for the effects of active rotation.

The numerical methods used to solve the model are discussed in chapter 3.

Chapter 4 describes different dynamical regimes predicted by our model. The numerical results are presented along with scaling arguments explaining numerical observations in different dynamical regimes.

Finally chapter 5 summarizes our current work and discusses the possible directions of future research in light of the questions that need to be answered.

Chapter 2

Model Dynamics

We consider a 50:50 mixture of two liquids where the components of each liquid phase are rotationally driven in opposite direction by an applied torque of constant magnitude (Figure 2.1). We assume that the two liquid phases are incompressible, Newtonian and "symmetric" such that the macroscopic properties of the two phases are equal – in particular, the density and viscosity. We further limit our analysis to 2D system in the *xy*-plane with active rotation in the *z*-direction. Physically the system can be thought to represent an ensemble of active particles moving and rotating above a planar substrate as is often the case in experimental realizations of active matter in 2D[33]. In order to develop the continuum model for describing phase separation in such binary system under active rotation first we start with theories of phase separation in passive system.

2.1 Coarsening Dynamics of Passive Binary Liquids

The seminal work on the coarsening of passive binary system after a rapid quench from a homogeneous phase into a two-phase region was done by Lifshitz, Slyozov[34] and Wagner[35] – more commonly known as LSW theory. The passive system can be thought of a 50:50 mixture of two incompressible, Newtonian and "symmetric" liquids. During phase of such system the local compositional field can be characterized by an order parameter φ. The value of order parameter is $\varphi = 0$ in single phase region where the two

liquids are homogeneously mixed and symmetric and equal to $\pm\varphi_{eq}$ in two-phase region where the domains of each liquid phase coarsen over time. The coarsening takes place such that the order parameter satisfies well known Cahn-Hilliard equation[36] –

$$\frac{\partial \varphi}{\partial t} = M\nabla^2 \mu \tag{2.1}$$

Where M is the mobility coefficient and μ is the chemical potential. The chemical potential can be written in the form[37,38]

$$\mu = -r\varphi + \lambda\varphi^3 - K\nabla^2\varphi \tag{2.2}$$

Here r , λ and K are positive coefficients. Physically these coefficients determine the thickness ($(K/r)^{1/2}$) of the interface between the two equilibrium phases $\varphi = \pm(r/\lambda)^{1/2}$. (2.1) applies to binary alloys, binary liquids and polymer blends given that the hydrodynamic flow can be neglected and the compositional field is governed by LSW theory – diffusive transport of material from regions of high interfacial curvature to regions of low curvature. In order to account for the effects of hydrodynamic flow in the binary liquids an additional convective term is added in (2.1) where the compositional field is coupled to the hydrodynamic flow as [37,38] –

$$\frac{\partial \varphi}{\partial t} + \nabla \cdot (\varphi \mathbf{v}) = M\nabla^2 \mu \tag{2.3}$$

(2.3) is also known as convective Cahn-Hilliard equation. Here $\mathbf{v}$ is the fluid velocity and the second term in (2.3) accounts for the advective transport of order parameter by

the fluid flow. Under the assumptions of incompressible and Newtonian liquid the conservation of mass and momentum imply that –

$$\nabla \cdot \mathbf{v} = 0 \tag{2.4}$$

$$\rho \frac{d\mathbf{v}}{dt} = -\nabla p + \eta \nabla^2 \mathbf{v} + \mu \nabla \varphi \tag{2.5}$$

Where ρ, η and p represent the density, viscosity and pressure respectively. The last term in (2.5) describes capillary forces acting at the interface between the two liquids[37,38].

2.2 Continuum Model for Actively Rotating Binary Liquids

Now we consider the active system of interest. The active rotation in each liquid phase is characterized by an applied torque density $\varphi\boldsymbol{\tau}$ which is proportional to the order parameter φ and to a constant vector $\boldsymbol{\tau}$ that describes the magnitude and direction of the rotation. For such system, the order parameter φ is governed by (2.3). However we assume that the velocity $\mathbf{v}$ arises due to the active rotation, neither induced by externally imposed flow nor due to the capillary forces in the system. Consequently, such active rotation induces an additional term in (2.5) of the form $\nabla \times (\varphi\boldsymbol{\tau})$, which gives rise to localized forces parallel to the interface[39]. To account for the frictional interactions between the particles and the underlying substrate, we introduce a final force term in (2.5) of the form $-b\mathbf{v}$, where b is the frictional coefficient such that the frictional drag force is proportional to the fluid flow. Thus active rotation induced flow is governed by –

$$\rho \frac{d\mathbf{v}}{dt} = -\nabla p + \eta \nabla^2 \mathbf{v} + \mu \nabla \varphi + \nabla \times (\varphi\boldsymbol{\tau}) - b\mathbf{v} \tag{2.6}$$

2.2.1 Non-dimensionalization

We non-dimensionalize the governing equations using characteristic scales for the interfacial thickness $(K/r)^{1/2}$, diffusive time scale K/Mr^2, the equilibrium composition $(r/\lambda)^{1/2}$ and the chemical potential $(r^3/\lambda)^{1/2}$. In dimensionless form, (2.3) and (2.6) reduce to

$$\frac{\partial \varphi}{\partial t} + \mathbf{v}\cdot\nabla\varphi = \nabla^2\left(-\varphi + \varphi^3 - \nabla^2\varphi\right) \tag{2.7}$$

$$Re\frac{d\mathbf{v}}{dt} = -\nabla p + \nabla^2\mathbf{v} + Ca^{-1}\mu\nabla\varphi + \alpha\nabla\times(\varphi\mathbf{e}_z) - \beta\mathbf{v} \tag{2.8}$$

Where $Re = \rho Mr/\eta$ is Reynolds number, $Ca = M\lambda\eta/K$ is a capillary number and $\alpha = \boldsymbol{\tau}K/\eta M(r^3\lambda)^{1/2}$ and $\beta = bK/\eta r$ are two dimensionless coefficients of the system characterizing the strength of active rotation compared to viscous damping and frictional drag compared to viscous damping, respectively. In this study we exclusively focus on the low Reynolds number limit (*i.e.* $Re \to 0$) and neglect capillary forces ($Ca^{-1} \to 0$) such that the fluid flow is driven solely by the active rotation of the particles. Under these conditions we can express (2.8) in terms of stream function ψ for the 2D system of interest (Appendix A) –

$$0 = \nabla^4\psi + \alpha\nabla^2\phi - \beta\nabla^2\psi \tag{2.9}$$

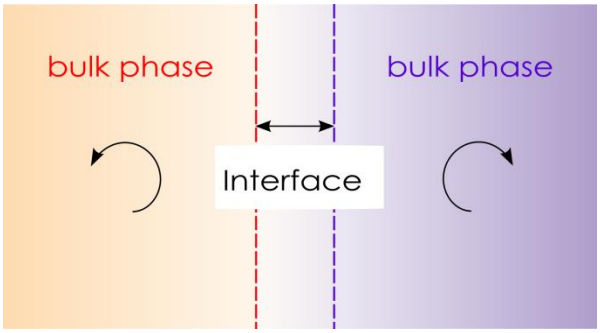

Figure 2.1 Schematic Diagram. The system consists of two symmetric liquid phases (purple and orange) separated by an interfacial region (white). The two phases are rotationally driven by an applied torque density in opposite direction.

Chapter 3

Methodology

3.1 Numerical Method

The governing equations are solved numerically on a square domain ($L \times L$) with periodic boundary conditions using semi-implicit Fourier spectral method[40] for different values of the two dimensionless parameters α and β . In Fourier space the governing equations become

$$\frac{\partial \Phi(\mathbf{k},t)}{\partial t} + \left(ik_x \{v_x \varphi\}_{\mathbf{k}} + ik_y \{v_y \varphi\}_{\mathbf{k}} \right) = -k^2 \{\varphi^3 - \varphi\}_{\mathbf{k}} - k^4 \Phi(\mathbf{k},t) \tag{3.1}$$

$$0 = k^4 \Psi(\mathbf{k},t) - \alpha k^2 \Phi(\mathbf{k},t) + \beta k^2 \Psi(\mathbf{k},t) \tag{3.2}$$

Where, $\mathbf{k} = (k_x, k_y)$ is a vector in the Fourier space with magnitude $k = (k_x^2 + k_y^2)^{1/2}$ and $\Phi(\mathbf{k},t)$ and $\Psi(\mathbf{k},t)$ are the Fourier transforms of compositional field $\varphi(\mathbf{r},t)$ and stream function $\psi(\mathbf{r},t)$ respectively. Rearranging (3.2) we compute stream function as

$$\Psi(\mathbf{k},t) = \frac{\alpha k^2}{(k^4 + \beta k^2)} \Phi(\mathbf{k},t) \tag{3.3}$$

The velocity field in the Fourier space can be computed as $V_x = ik_y \psi$ and $V_y = -ik_x \psi$; the velocity is then obtained by taking the inverse Fourier transform.

3.1.1 Time Stepping

First-order semi-implicit Fourier spectral scheme results in following equation:

$$\left(1+\Delta t k^4\right)\Phi^{n+1} = \Phi^n - \Delta t k^2 \{\varphi^3 - \varphi\}_{\mathbf{k}}^n - \Delta t \left(ik_x \{v_x \varphi\}_{\mathbf{k}}^n + ik_y \{v_y \varphi\}_{\mathbf{k}}^n\right) \tag{3.4}$$

If we write the non-linear terms $\{\varphi^3 - \varphi\}_{\mathbf{k}}^n$ and $\left(ik_x \{v_x \varphi\}_{\mathbf{k}}^n + ik_y \{v_y \varphi\}_{\mathbf{k}}^n\right)$ as $\{f_1(\varphi^n)\}_{\mathbf{k}}$ and $\{f_2(v^n, \varphi^n)\}_{\mathbf{k}}$ respectively, (3.4) becomes:

$$\left(1+\Delta t k^4\right)\Phi^{n+1} = \Phi^n - \Delta t \left(k^2 \{f_1(\varphi^n)\}_{\mathbf{k}} + \{f_2(v^n, \varphi^n)\}_{\mathbf{k}}\right) \tag{3.5}$$

For improved accuracy in time, higher order semi-implicit scheme of second-order Adams-Bashforth/Backward-differentiation (AB2/BDF2) method results in:

$$\begin{aligned} &\left(3+2\Delta t k^4\right)\Phi^{n+1} = 4\Phi^n - \Phi^{n-1} \\ &-2\Delta t \left[2\left(k^2 \{f_1(\varphi^n)\}_{\mathbf{k}} + \{f_2(v^n, \varphi^n)\}_{\mathbf{k}}\right) - \left(k^2 \{f_1(\varphi^{n-1})\}_{\mathbf{k}} + \{f_2(v^{n-1}, \varphi^{n-1})\}_{\mathbf{k}}\right)\right] \end{aligned} \tag{3.6}$$

(3.5) is used for initializing the iteration in (3.6).

3.2 Computer Simulation

Initially, the system is prepared in a homogeneous state such that the composition at each lattice site is assigned from the interval $[-0.1, 0.1]$ at random. Depending on the strength of active rotation (α) and frictional damping compared to viscous damping (β) in the system our model exhibits a rich variety of phase behaviors ranging from diffusive coarsening to dynamic coarsening by "vortex-doublets". Same initial state is used for all regimes with spatial mesh size $(\Delta x, \Delta y) = (1,1)$. All simulations are performed using Matlab on Intel Xeon X5675 Six-Core 3.06 GHz processors that are part of the lionXF and lion-GA (equipped with Nvidia Quadro 2000 GPU hardware) clusters run by High Performance Computing Group of The Pennsylvania State University. In the next chapter the phase diagram is presented and each qualitatively distinct regime is discussed in turn. Detailed scaling arguments are provided also to explain the behaviors observed numerically.

Chapter 4

Results and Discussions

4.1 Passive System

The coarsening dynamics of the Cahn-Hilliard model without active rotation have been studied previously in great detail[36]. At short times ($t \ll 1$), the initially homogeneous state undergoes an instability characterized by a wavenumber $k = 2^{-1/2}$, which grows in time at a rate $\frac{1}{4}$ until the formation of bulk domains with $\varphi \approx \pm 1$ separated by an interfacial region of unit thickness (Appendix B). At longer times ($t \gg 1$), these domains grow in size as $R \sim t^{1/3}$ due to small composition gradients ($\Delta\varphi \sim R^{-1}$) which drive diffusive fluxes ($j \sim \Delta\varphi / R$) that act to grow the domains ($dR/dt \sim j$) and reduce the curvature of the interface.

4.2 Active System

4.2.1 Phase Diagram

We studied the role of the strength of active rotation (α) and frictional damping relative to viscous damping (β) on system's macroscopic dynamics. Our model predicts a rich variety of phase behavior in the active system (Figure 4.1). When the frictional damping is dominant compared to viscous damping in the system it is considered to be in the strong damping regime ($\beta \gg 1$). In addition to recovering the passive coarsening under the conditions of weak rotation ($\alpha \ll \beta$) as observed in case of spinners, our

model suggests passive coarsening in case of strong rotation ($\alpha \gg \beta$) also in strong damping regime. Moreover, it predicts several new types of phase behavior such as accelerated active coarsening and emergence of vortex doublet in weak damping regime($\beta \ll 1$) where the frictional damping is weak compared to that by viscous coupling. Figure 4.1 provides an overview of different dynamical regimes along with their characteristic morphological pattern.

4.2.2 Strong Damping

For strong frictional damping ($\beta \gg 1$), forces due to active rotation are everywhere balanced by frictional drag; the dominant terms of (2.8) are $\alpha \nabla \times (\varphi \mathbf{e}_z) \approx \beta \mathbf{v}$ (see detail in Appendix B). The domain size increases as $R \sim t^{1/3}$ independent of both α and β in quantitative agreement with passive diffusive coarsening (Figure 4.2). However unlike passive system, there is a rotation induced flow parallel to the interface between the two bulk phases. The flow is confined largely within interfacial region due to strong frictional damping and the characteristic velocity scales as $U \sim \alpha / \beta$. Within this region the gradients in the order parameter are of order unity. Fluid flows are directed perpendicular to gradients in the order parameter, such that $\mathbf{v} \cdot \nabla \varphi \approx 0$. Consequently, these flows do not significantly influence the evolution of the order parameter regardless of the magnitude of active rotation.

4.2.3 Weak Damping

We further investigate the system for weak frictional damping ($\beta \ll 1$) where the active driving force is balanced mainly by the viscous damping. In this case the dominant terms of (2.8) are $\alpha \nabla \times (\varphi \mathbf{e}_z) \approx \nabla^2 \mathbf{v}$. Due to the weak frictional damping, the rotation induced flow is no more confined within interface only, rather the velocity of the liquid drops gradually from a maximum at the center of the interface to zero in the bulk phase within a flow region characterized by $l \sim \beta^{-1/2}$. Unlike strong damping regime, several new types of dynamics are observed in weak damping regime. First of all we investigate the system under weak rotation ($\alpha \ll \beta$). The characteristic velocity in this regime scales as $U \sim \alpha / \beta^{1/2}$ such that the Peclet number is much smaller than one ($Pe < 1$). Here, the Peclet number is defined as $Pe = Ul$; with U as the characteristic velocity and l as the characteristic length scale of the flow region. Thus diffusion plays the dominant transport mechanism under weak rotation. Consequently, the system coarsens by diffusion and the domain size grows in time as $R \sim t^{1/3}$ similar to the passive system (Figure 4.3). In case of strong rotation ($\alpha \gg \beta$) three stages of coarsening are observed – (i) early stage of diffusive coarsening, (ii) intermediate stage of active coarsening, and finally (iii) late stage of diffusive coarsening. At early time, the characteristic velocity ($U \sim \alpha R$) depends on the domain size. The Peclet number ($Pe = \alpha R^2$) during this time is small ($Pe < 1$) such that the coarsening dynamics is diffusion-controlled. As the domain size ($\alpha^{-1/2} < R < \beta^{-1/2}$) grows in time, the Peclet number gradually becomes large ($Pe > 1$). Consequently, convection becomes dominant compared to diffusion and the system starts to deviate from the passive coarsening. During this intermediate stage the system

exhibits accelerated active coarsening as compared to the passive system (Figure 4.3). At even late stage, the velocity turns out to be independent of the domain size and scales as $U \sim \alpha / \beta^{1/2}$. At this point the domain size R is much larger than the flow region ($R > \beta^{-1/2}$). Therefore diffusion plays the role of the dominant transport mechanism again and the domain size grows as $R \sim t^{1/3}$.

4.2.3.1 Zero damping

Interestingly, no dynamic scaling is observed during the short-lived intermediate stage of active coarsening. In order to investigate active coarsening in more details, we study the system in the limit of zero frictional damping in the system ($\beta \to 0$) such that late stage diffusive coarsening is never observed in a finite system since the flow region will always be larger compared to the domain size. The active driving force is solely balanced by the viscous damping in such system. Under this condition following the early stage of diffusive coarsening, accelerated active coarsening continues indefinitely. A closer inspection of the morphological pattern reveals that instead of a single characteristic domain size, a spectrum of characteristic length scales emerge in the system (Figure 4.4a). Interestingly, some of these length scales appear to remain frozen while others are coarsening over time. Qualitatively, the morphological pattern in this regime looks similar to that observed in case of coarsening under stirring condition[41]. In such system filamental structures appear that becomes arrested at long time. Interestingly, in addition to arrested filamental structures seem an overall coarsening of the larger length scales is also observed in the active system. It is important note here that these comments are made upon visual inspection of the active system.

4.2.3.2 Vortex-doublet

At even higher active rotation ($\alpha \gg 1$) with zero frictional damping ($\beta \to 0$) in the system, active droplets nucleate within a homogeneously mixed liquid phase (Figure 4.4b). The chaotic flow arising from active rotation prevents demixing of the liquids in most regions while active droplets nucleate in the regions of low shear. Following the nucleation period, the active droplets grow heterogeneously by merging in pair with other like-rotating active droplets. During this coalescence period, the number of active droplets in the system decreases with time as the coalescence dominates over formation of new nuclei (Figure 4.5). Any further nucleation is prevented in the vicinity of the large active droplets due the high shear around it. At longer time "vortex-doublets", pair of oppositely rotating active droplets, emerge in the system. Preliminary results suggest that the number of active droplets (N) present in the system at a given time is a function of both active rotation and the system size (L) such that $N \propto 1/L^2$ and $N \propto \alpha$. The characteristic velocity (U) in this regime depends on both the gradient of order parameter and domain size and scales as $U \sim \alpha R \Delta\phi$. The convection becomes dominant ($Pe > 1$) even before formation of the fully phase separated liquid phases unlike any other regimes, thus preventing full phase separation.

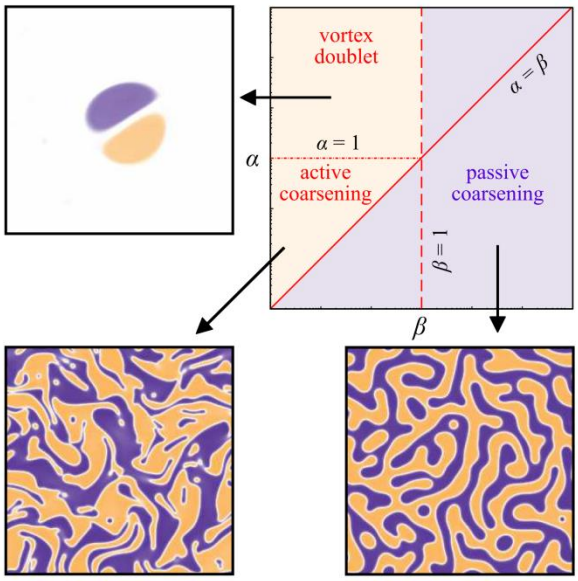

Figure 4.1 Phase Diagram. α measures the strength of active rotation and β measures the strength of frictional damping compared to viscous damping in the system. Regimes exhibiting *passive coarsening* are shaded in purple and regimes exhibiting *active coarsening* and *vortex doublets* are shaded in orange. Representative morphological patterns are shown for each dynamical regime. $\beta \gg 1$ corresponds to *strong damping* regime and $\beta \ll 1$ corresponds to *weak damping* regime. The system is under strong rotation for $\alpha \gg \beta$ and vice versa.

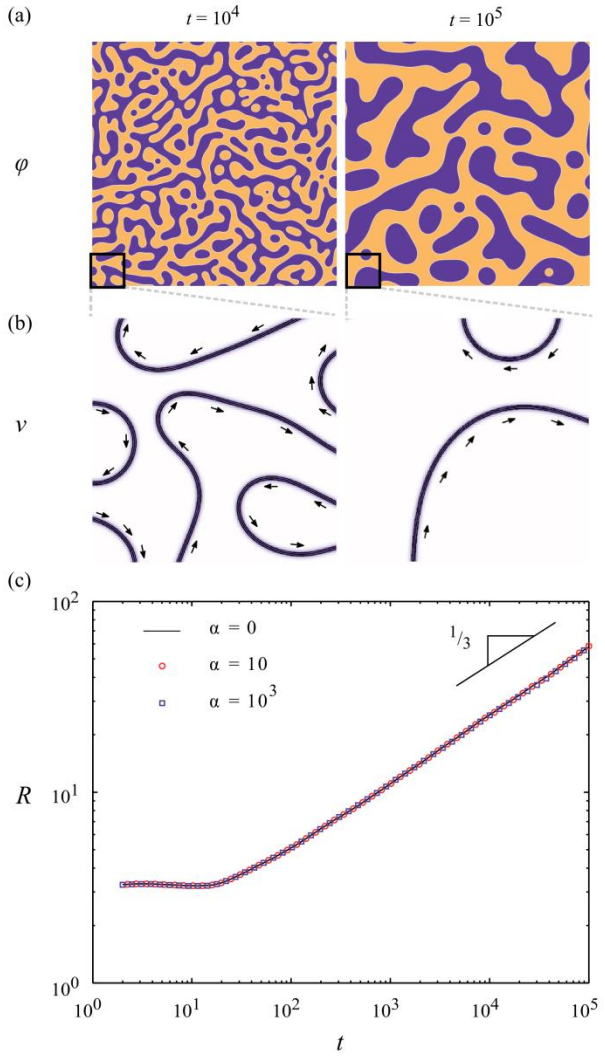

Figure 4.2 Strong Damping. (a) Order parameter $\varphi(x, y)$ at times $t = 10^4$ and $t = 10^5$ for parameters $\alpha = 10$ and $\beta = 10^2$; the size of simulation cell is $L = 1024$ with $\Delta x = \Delta y = 1$. (b) Velocity field $\mathbf{v}(x, y)$ corresponding to the insets in (a). Arrows show direction of local velocity field. (c) Domain size, R as a function of time for $\beta = 10^2$ and $\alpha = 0$, 10 and 10^3; the domain size, R is defined as the first zero of the radial pair correlation function, $g(R) = 0$. The solid black line shows the expected scaling exponent of $1/3$.

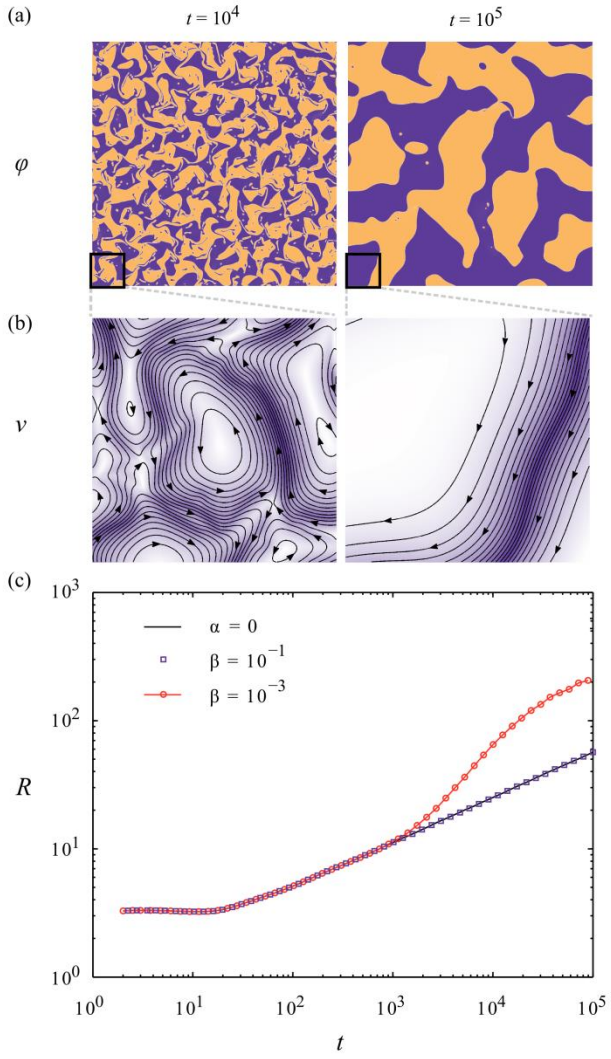

Figure 4.3 Weak damping. (a) Order parameter $\varphi(x, y)$ at times $t = 10^4$ and $t = 10^5$ for parameters $\alpha = 0.01$ and $\beta = 10^{-3}$; the size of simulation cell is $L = 2048$ with $\Delta x = \Delta y = 1$. (b) Velocity field $\mathbf{v}(x, y)$ corresponding to the insets in (a). Arrows show direction of local velocity field. (c) Domain size, R as a function of time for passive ($\alpha = 0$) and active ($\alpha = 0.01$) systems at different damping coefficients ($\beta = 10^{-1}$ and 10^{-3}).

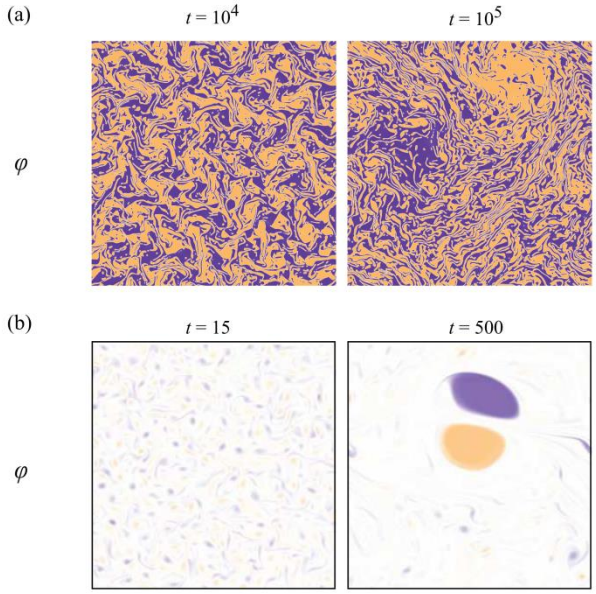

Figure 4.4 Morphological Evolution**.** (a) Order parameter $\varphi(x, y)$ at times $t = 10^4$ and $t = 10^5$ for parameters $\alpha = 0.01$ and $\beta \to 0$; the size of simulation cell is $L = 2048$ with $\Delta x = \Delta y = 1$. Multiple length scales emerge in the system. (b) Order parameter $\varphi(x, y)$ at times $t = 15$ and $t = 500$ for parameters $\alpha = 50$ and $\beta \to 0$; the size of simulation cell is $L = 256$ with $\Delta x = \Delta y = 1$. At early time active droplets (in purple and orange) nucleate within homogeneously mixed fluid phase (white). At longer time "vortex-doublets" – pair of oppositely rotating active droplets emerge in the system as in case of $t = 500$.

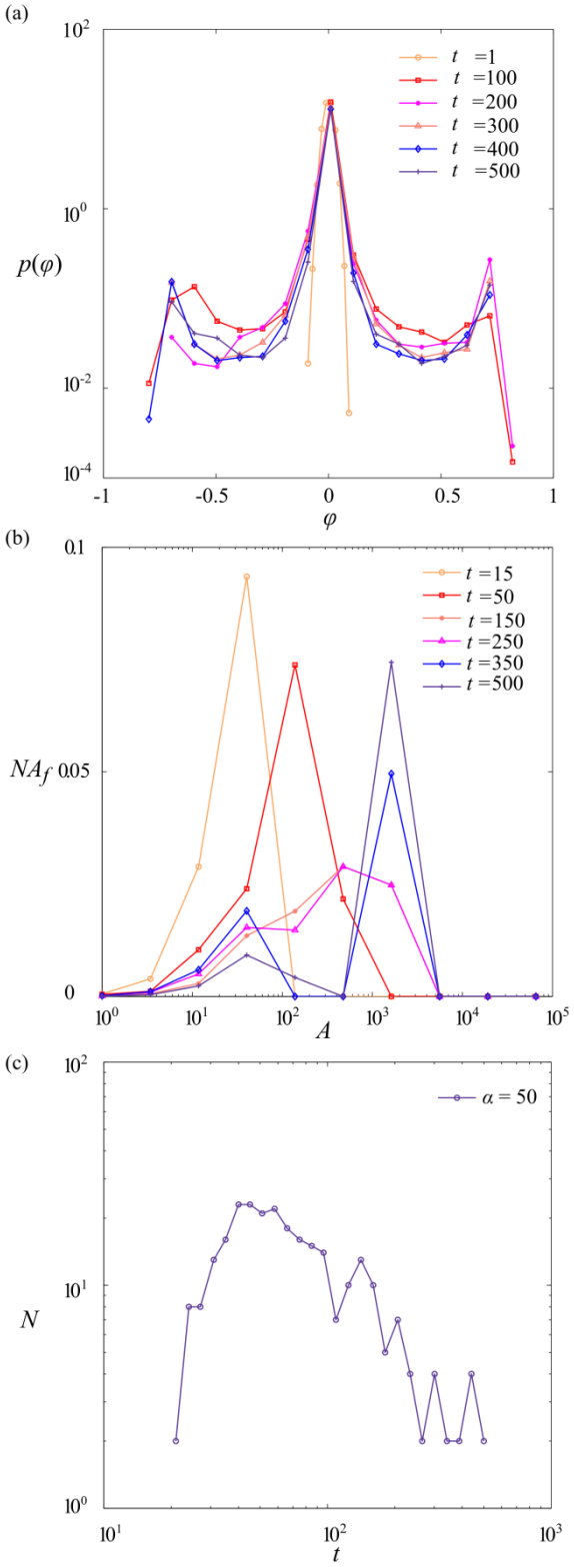
(a)
10^2
10^0
10^{-2}
10^{-4}
$p(\varphi)$
-1
-0.5
0
0.5
1
φ
t =1
t =100
t =200
t =300
t =400
t =500
(b)
0.1
0.05
0
NA_f
10^0
10^1
10^2
10^3
10^4
10^5
A
t =15
t =50
t =150
t =250
t =350
t =500
(c)
10^2
10^1
10^0
N
10^1
10^2
10^3
t
$\alpha = 50$

Figure 4.5 Vortex-Doublets. (a) Distribution of order parameter $\varphi(x, y)$ at different times for parameters $\alpha = 50$ and $\beta \to 0$. The peak around $\varphi = 0$ corresponds to the mixed fluid phase and the symmetric peaks around $\varphi = \pm 0.8$ correspond to the active droplets present in the system. (b) Area distribution of the active droplets at different times for $\alpha = 50$ and $\beta \to 0$. The bimodal distribution at longer time corresponds to the coexistence of relatively large vortex-doublets and newly formed active nuclei in the system. (c) Number of active droplets (*N*) as a function time for $\alpha = 50$ and $\beta \to 0$.

Chapter 5

Conclusions

In summary, the continuum model predicts a rich variety of phase behaviors in binary liquids under active rotation as anticipated. It demonstrates several new dynamical regimes for the active system. In addition to diffusion-controlled coarsening, the model suggests accelerated active coarsening as well as formation of vortex-doublets in weak damping regime. This model thus enriches our fundamental understanding of emergent collective behaviors in ensembles of actively rotating particles. The continuum model will further inform and guide the experimental realization of the system.

5.1 Remaining questions

Despite current understanding of different dynamical regimes there are still some questions that need be answered in order to provide more insights about the collective dynamics of the actively rotating system. Preliminary observations for zero damping system ($\beta \to 0 ; \alpha < 1$) suggest that, although fully phase separated domains are formed but instead of single characteristic domain size, multiple length scales emerge in the system. It is important to answer which of these length scales are important for characterizing the coarsening in this regime. In order to do so first we need to identify these different length scales present in the system. The next question is whether it is necessary to describe domain morphology with more than one length-scale. Even if there are multiple length scales it may still be possible to provide a complete description of dynamic scaling (if exists) based on the most important one, once identified. Based on the

visual observation of the system's morphology in this regime, two length scales seems to be most important – the smallest one that seems to remain unchanged over time and the largest one that coarsens over time. It is also important to understand the relative importance of these length scales in relation to the strength of active rotation. In order to identify multiple length scales, dynamic structure factor may be used. Image analysis procedure may also be useful in order to verify what is observed through the results of structure factor analysis.

On the other hand, it is computationally challenging to simulate long term behavior of large systems in vortex-doublet regime. Although the nucleation period and growth period in this regime can be identified, it is not fully characterized yet how the nucleation rate as well as coalescence rate depends on the strength of active rotation and the system size rather than some qualitative understanding. Preliminary observations suggest that the chaotic flow profile arising from the strong active rotation gives rise to mixed fluid phase and nuclei form in the pockets of low shear. However, it would be more compelling to understand the relation between the local shear rates with the nucleation rate at different levels of active rotation. Once the role of active rotation and system size on nucleation rate and the following growth process can be described in more quantitative fashion, it can guide our prediction about long term behavior for the system.

Bibliography

1. Nguyen, N. H. P., Klotsa, D., Engel, M. & Glotzer, S. C. Emergent Collective Phenomena in a Mixture of Hard Shapes through Active Rotation. *Phys. Rev. Lett.* **112,** 075701 (2014).

2. Marchetti, M. C. *et al.* Hydrodynamics of soft active matter. *Rev. Mod. Phys.* **85,** 1143–1189 (2013).

3. Sanchez, T., Chen, D. T. N., DeCamp, S. J., Heymann, M. & Dogic, Z. Spontaneous motion in hierarchically assembled active matter. *Nature* **491,** 431–4 (2012).

4. Vicsek, T. & Zafeiris, A. Collective motion. *Phys. Rep.* **517,** 71–140 (2012).

5. Dreyfus, R. *et al.* Microscopic artificial swimmers. *Nature* **437,** 862–865 (2005).

6. Khatavkar, V. V., Anderson, P. D., den Toonder, J. M. J. & Meijer, H. E. H. Active micromixer based on artificial cilia. *Phys. Fluids* **19,** 083605 (2007).

7. Arco, R. M., Vélez-Cordero, J. R., Lauga, E. & Zenit, R. Viscous pumping inspired by flexible propulsion. *Bioinspir. Biomim.* **9,** 036007 (2014).

8. Chen, A. Y. *et al.* Synthesis and patterning of tunable multiscale materials with engineered cells. *Nat. Mater.* **13,** 515–23 (2014).

9. Nguyen, N. H. P., Jankowski, E. & Glotzer, S. C. Thermal and athermal three-dimensional swarms of self-propelled particles. *Phys. Rev. E* **86,** 011136 (2012).

10. Peruani, F., Deutsch, A. & Bär, M. Nonequilibrium clustering of self-propelled rods. *Phys. Rev. E* **74,** 030904 (2006).

11. Jelsbak, L. & Søgaard-Andersen, L. Pattern formation: fruiting body morphogenesis in Myxococcus xanthus. *Curr. Opin. Microbiol.* **3,** 637–42 (2000).

12. Koch, D. L. & Subramanian, G. Collective Hydrodynamics of Swimming Microorganisms: Living Fluids. *Annu. Rev. Fluid Mech.* **43,** 637–659 (2011).

13. Angelani, L., Di Leonardo, R. & Ruocco, G. Self-starting micromotors in a bacterial bath. *Phys. Rev. Lett.* **102,** 048104 (2009).

14. Sokolov, A., Apodaca, M. M., Grzybowski, B. A. & Aranson, I. S. Swimming bacteria power microscopic gears. *Proc. Natl. Acad. Sci. U. S. A.* **107,** 969–974 (2010).

15. Sokolov, A. & Aranson, I. Reduction of Viscosity in Suspension of Swimming Bacteria. *Phys. Rev. Lett.* **103,** 148101 (2009).

16. Sokolov, A., Goldstein, R., Feldchtein, F. & Aranson, I. Enhanced mixing and spatial instability in concentrated bacterial suspensions. *Phys. Rev. E* **80,** 031903 (2009).

17. Wang, W., Duan, W., Sen, A. & Mallouk, T. E. Catalytically powered dynamic assembly of rod-shaped nanomotors and passive tracer particles. *Proc. Natl. Acad. Sci. U. S. A.* **110,** 17744–9 (2013).

18. Blair, D., Neicu, T. & Kudrolli, A. Vortices in vibrated granular rods. *Phys. Rev. E* **67,** 031303 (2003).

19. Toyota, T., Maru, N., Hanczyc, M. M., Ikegami, T. & Sugawara, T. Self-propelled oil droplets consuming "fuel" surfactant. *J. Am. Chem. Soc.* **131,** 5012–3 (2009).

20. Vicsek, T., Czirok, A., Ben-Jacob, E., Cohen, I. & Shochet, O. Novel type of phase transition in a system of self-driven particles. *Phys. Rev. Lett.* **75,** 1226–1229 (1995).

21. Grzybowski, B., Stone, H. & Whitesides, G. Dynamic self-assembly of magnetized, millimetre-sized objects rotating at a liquid-air interface. *Nature* **405,** 1033–6 (2000).

22. Schwarz-Linek, J. *et al.* Phase separation and rotor self-assembly in active particle suspensions. *Proc. Natl. Acad. Sci. U. S. A.* **109,** 4052–7 (2012).

23. Uchida, N. & Golestanian, R. Synchronization and collective dynamics in a carpet of microfluidic rotors. *Phys. Rev. Lett.* **104,** (2010).

24. Grzybowski, B. A. & Whitesides, G. M. Dynamic aggregation of chiral spinners. *Science* **296,** 718–21 (2002).

25. Drescher, K. *et al.* Dancing volvox: Hydrodynamic bound states of swimming algae. *Phys. Rev. Lett.* **102,** (2009).

26. Darnton, N., Turner, L., Breuer, K. & Berg, H. C. Moving fluid with bacterial carpets. *Biophys. J.* **86,** 1863–1870 (2004).

27. Roeller, K., Clewett, J. P. D., Bowley, R. M., Herminghaus, S. & Swift, M. R. Liquid-Gas Phase Separation in Confined Vibrated Dry Granular Matter. *Phys. Rev. Lett.* **107,** 048002 (2011).

28. Liu, Q.-X. *et al.* Phase separation explains a new class of self-organized spatial patterns in ecological systems. *Proc. Natl. Acad. Sci. U. S. A.* **110,** 11905–10 (2013).

29. Theurkauff, I., Cottin-Bizonne, C., Palacci, J., Ybert, C. & Bocquet, L. Dynamic Clustering in Active Colloidal Suspensions with Chemical Signaling. *Phys. Rev. Lett.* **108,** 268303 (2012).

30. Fily, Y. & Marchetti, M. C. Athermal Phase Separation of Self-Propelled Particles with No Alignment. *Phys. Rev. Lett.* **108,** 235702 (2012).

31. Fily, Y., Henkes, S. & Marchetti, M. C. Freezing and phase separation of self-propelled disks. *R. Soc. Chem.* 2132–2140 (2014). doi:10.1039/c3sm52469h

32. Redner, G. S., Baskaran, A. & Hagan, M. F. Reentrant phase behavior in active colloids with attraction. *Phys. Rev. E* **88,** 012305 (2013).

33. Redner, G. S., Baskaran, A. & Hagan, M. F. Reentrant phase behavior in active colloids with attraction. *Phys. Rev. E* **88,** 012305 (2013).

34. Lifshitz, I. M. & Slyozov, V. V. The kinetics of precipitation from supersaturated solid solutions. *J. Phys. Chem. Solids* **19,** 35–50 (1961).

35. Wagner, C. Theorie der Alterung von Niederschlägen durch Umlösen. *Zeitschrift für Elektrochemie* **65,** 581–591 (1961).

36. Bray, A. J. Coarsening dynamics of phase-separating systems. *Philos. Trans. A. Math. Phys. Eng. Sci.* **361,** 781–91; discussion 791–2 (2003).

37. Jasnow, D. & Vin, J. Coarse-grained description of thermo-capillary flow. *Phys. Fluids* **8,** 660–669 (1996).

38. Anderson, D. M., McFadden, G. B. & Wheeler, A. A. Diffuse-Interface Methods in Fluid Mechanics. *Annu. Rev. Fluid Mech.* **30,** 139–165 (1998).

39. Rosensweig, R. E. Continuum equations for magnetic and dielectric fluids with internal rotations. *J. Chem. Phys.* **121,** 1228–42 (2004).

40. Zhu, J., Chen, L. Q., Shen, J. & Tikare, V. Coarsening kinetics from a variable-mobility Cahn-Hilliard equation: application of a semi-implicit Fourier spectral method. *Phys. Rev. E* **60,** 3564–3572 (1999).

41. Berti, S., Boffetta, G., Cencini, M. & Vulpiani, A. Turbulence and Coarsening in Active and Passive Binary Mixtures. *Phys. Rev. Lett.* **95,** 224501 (2005).

Appendices

A. Formulation of Stream Function

According to the definition of stream function we may write –

$$\mathbf{v} = \nabla \times (\psi \mathbf{e}_z) = \frac{\partial \psi}{\partial y}\mathbf{e}_x - \frac{\partial \psi}{\partial x}\mathbf{e}_y \tag{A.1}$$

It is convenient to express (2.8) in terms of stream function ψ for the two dimensional active system.

$$0 = -\frac{\partial P}{\partial x} + \left(\frac{\partial^3 \psi}{\partial x^2 \partial y} + \frac{\partial^3 \psi}{\partial y^3} \right) + \alpha \frac{\partial \varphi}{\partial y} - \beta \frac{\partial \psi}{\partial y} \tag{A.2}$$

$$0 = -\frac{\partial P}{\partial y} - \left(\frac{\partial^3 \psi}{\partial x^3} + \frac{\partial^3 \psi}{\partial x \partial y^2} \right) - \alpha \frac{\partial \varphi}{\partial x} + \beta \frac{\partial \psi}{\partial x} \tag{A.3}$$

(A.2) and (A.3) are *x* and *y* – components of (2.8) under the assumption of low Reynolds number and negligible capillary force. Differentiating (A.2) by *y* and (A.3) by *x* and subtracting the resulting equations we find

$$0 = \left(\frac{\partial^4 \psi}{\partial x^4} + 2\frac{\partial^4 \psi}{\partial x^2 \partial y^2} + \frac{\partial^4 \psi}{\partial y^4} \right) + \alpha \left(\frac{\partial^2 \varphi}{\partial y^2} + \frac{\partial^2 \varphi}{\partial x^2} \right) - \beta \left(\frac{\partial^2 \psi}{\partial x^2} + \frac{\partial^2 \psi}{\partial y^2} \right) \tag{A.4}$$

$$0 = \nabla^4 \psi + \alpha \nabla^2 \varphi - \beta \nabla^2 \psi \tag{A.5}$$

B. Dominant Balance Analysis

The dimensionless governing equations for the order parameter $\phi(\mathbf{r},t)$ and the stream function $\psi(\mathbf{r},t)$ are

$$\frac{\partial \varphi}{\partial t} + \mathbf{v}\cdot\nabla\varphi = \nabla^2(\varphi^3 - \varphi - \nabla^2\varphi) \tag{B.1}$$

$$0 = \nabla^4\psi + \alpha\nabla^2\varphi - \beta\nabla^2\psi \tag{B.2}$$

where the velocity is $\mathbf{v} = \nabla\times(\psi\mathbf{e}_z)$.

B.1. Passive System

In the absence of active rotation, the convective velocity is zero and (B.1) simplifies to the Cahn-Hilliard equation,

$$\frac{\partial \varphi}{\partial t} = \nabla^2(\varphi^3 - \varphi - \nabla^2\varphi) \tag{B.3}$$

In early time ($t \ll 1$) the system is (nearly) homogeneous $\phi \approx 0$. Linearizing (B.3) about the homogeneous state gives

$$\frac{\partial \varphi}{\partial t} = -\nabla^2(\varphi + \nabla^2\varphi) \tag{B.4}$$

Assuming solution of the form,

$$\varphi(\mathbf{r},t) = \mathrm{Re}\left[\tilde{\varphi}(\mathbf{k},t)e^{i\mathbf{k}\cdot\mathbf{r}}\right] \tag{B.5}$$

Equation (B.4) can be written in Fourier space as –

$$\frac{\partial \tilde{\varphi}}{\partial t} = (k^2 - k^4)\tilde{\varphi} \tag{B.6}$$

where $k^2 = k_x^2 + k_y^2$. This result implies that small wavelength disturbances ($k > 1$) decay in time, whereas long wavelength disturbances ($k < 1$) grow in time. Here, $(k^2 - k^4)$ is dimensionless rate for the growth of disturbances and it is maximum at $k = 2^{-1/2}$. In particular, the dimensionless rate corresponding to fastest growing mode is $¼$. In other words, the early stages of phase separation proceed over times of order unity on a characteristic scale also of order unity.

At longer time ($t \gg 1$) there is sharp interfaces between the phase separated bulk phases and the domains begin to coarsen. In order to understand the process it is important to consider the system's dynamics within the two key regions: (*i*) the bulk and (*ii*) the interface.

Bulk. Within the bulk of either phase the order parameter is $\varphi \approx \pm 1$. Linearizing the governing equation (B.3) about $\varphi = 1$ gives

$$\frac{\partial \varphi}{\partial t} = \nabla^2(2\varphi - \cancel{\nabla^2\varphi}) \tag{B.7}$$

The term neglected here is found to be small in the bulk phase. Consequently, transport in the bulk phase obeys simple diffusion equation

$$\frac{\partial \varphi}{\partial t} = 2\nabla^2\varphi \tag{B.8}$$

Flat Equilibrium Interface. In order to understand the interfacial region first a one-dimensional problem of "flat" interface is considered where the compositional field changes along *x*-direction only. The interface is normal to the direction of gradients in compositional field and the governing equation (B.3) simplifies to

$$\frac{\partial \varphi}{\partial t} = \frac{\partial^2}{\partial x^2}\left((\varphi^3 - \varphi) - \frac{\partial^2 \varphi}{\partial x^2} \right) \tag{B.9}$$

The temporal variation of order parameter in the interfacial region can neglected at long times. Integrating with respect to *x* twice and noting that $\varphi(\pm\infty) \to \pm 1$, yields

$$\frac{\partial^2 \varphi}{\partial x^2} = \varphi^3 - \varphi \tag{B.10}$$

For large $x \gg 1$, (B.10) can be approximated as

$$\frac{\partial^2 \varphi}{\partial x^2} = 2(\varphi - 1) \tag{B.11}$$

Solving (B.11) for compositional field gives

$$\varphi(x) = 1 - Ce^{-\sqrt{2}x} \tag{B.12}$$

Where *C* is a constant of order one. Using this asymptotic result (B.10) can be readily integrated numerically on a finite domain $0 \le x \le x_{\max}$ where $x_{\max} \gg 1$, using the boundary conditions

$$\phi(0) = 0 \text{ and } \left(\frac{1}{\sqrt{2}} \frac{d\varphi}{dx} + \varphi \right)_{x_{\max}} = 1 \tag{B.13}$$

The resulting solution is illustrated in Figure B.1. The constant C is estimated to be C = 2.

Flat Nonequilibrium Interface. What if the concentration in the bulk phases are not exact ± 1? Neglecting time derivative (B.3) can be written in one-dimension as

$$0 = \frac{\partial^2}{\partial x^2}\left((\varphi^3 - \varphi) - \frac{\partial^2 \varphi}{\partial x^2} \right) \tag{B.14}$$

Integrating once gives

$$j = \frac{\partial}{\partial x}\left((\varphi^3 - \varphi) - \frac{\partial^2 \varphi}{\partial x^2} \right) \tag{B.15}$$

where $j \neq 0$ is the constant flux across the interface. This flux of material across the interface must invariably cause the interface to move. In particular, if $\phi(-\infty) \approx 1$ and $\phi(\infty) \approx -1$, then a flux of in the negative x-direction will result in the movement of the interface at a velocity $U \sim j$ in the opposite direction. This physical reasoning suggests the introduction of a new coordinate system moving with a velocity U. Let X be such a moving coordinate defined as

$$X(x,t) = x + Ut \tag{B.16}$$

In the moving coordinate, the order parameter $\varphi(X,t)$ is governed by

$$\frac{\partial \varphi}{\partial t} = \frac{\partial^2}{\partial X^2}\left((\varphi^3 - \varphi) - \frac{\partial^2 \varphi}{\partial X^2} \right) - U \frac{\partial \varphi}{\partial X} \tag{B.17}$$

Again, the temporal variation of order parameter can be neglected at long times. Integrating once, the flux in the moving coordinate is given by

$$J = \frac{\partial}{\partial X}\left((\varphi^3 - \varphi) - \frac{\partial^2 \varphi}{\partial X^2} \right) - U\varphi \tag{B.18}$$

where U is chosen such that $J = 0$. Therefore (B.18) reduces to

$$\frac{\partial}{\partial X}\left((\varphi^3 - \varphi) - \frac{\partial^2 \varphi}{\partial X^2} \right) - U\varphi = 0 \tag{B.19}$$

Far from the interface ($|x| \gg 1$), (B.17) must simplify to

$$\frac{\partial \varphi}{\partial t} = 2\frac{\partial^2 \varphi}{\partial X^2} - U\frac{\partial \varphi}{\partial X} \tag{B.20}$$

Within the bulk regions, this flux is approximated as

$$j \approx -\frac{\partial}{\partial x}\big(2(\varphi - 1)\big) = -2\frac{\partial \varphi}{\partial x} \text{ for } |x| \gg 1 \tag{B.21}$$

B.2 Active System

In active system the velocity field is induced by the active rotation such that stream function formulation satisfies (B.2). For convenience, this can be rewritten for velocity in dimensional form.

$$0 = \eta \frac{\partial^2 v_x}{\partial y^2} + \tau \frac{\partial \phi}{\partial y} - b v_x \tag{B.22}$$

(B.22) is written for the *x*-component.

B.2.1. Strong Damping

Now, consider momentum damping by frictional drag force is dominant compared to that by viscous coupling. Due to strong frictional damping with the underlying substrate the velocity induced by the active rotation is mostly confined within the interface and drops to zero in the bulk phase (Figure B.2). Since there is a momentum source along the interface the dominant two terms in (B.22) for interfacial region –

$$\tau \frac{\Delta \varphi}{\Delta y} \sim b v_x \tag{B.23}$$

(B.23) can be written in dimensionless form –

$$\frac{\tau r}{(K\lambda)^{1/2}} \frac{\Delta \tilde{\varphi}}{\Delta \tilde{y}} \sim U \frac{bMr^{3/2}}{K^{1/2}} \text{ -} \tag{B.24}$$

Here, U, $\Delta\tilde{\varphi}$ and $\Delta\tilde{y}$ are characteristic velocity, order parameter and characteristic length scale respectively in dimensionless form. In interfacial region, $\Delta\tilde{\varphi} \sim 1$ and $\Delta\tilde{y} \sim 1$. Thus (B.24) reduces to-

$$U \sim \frac{\tau}{bM(r\lambda)^{1/2}} \sim \frac{\alpha}{\beta} \tag{B.25}$$

Since the viscous damping term would be negligible compared to the frictional drag term in (B.22)–

$$\eta \frac{v_x}{(\Delta y)^2} \ll b v_x \tag{B.26}$$

In dimensionless form (B.26) can be written as –

$$\frac{\eta r}{K(\Delta \tilde{y})^2} \ll b \tag{B.27}$$

Hence, this dynamical regime can be realized when

$$\beta \gg 1 \tag{B.28}$$

B.2.1. Weak Damping

Now consider that the viscous damping is dominant compared to the frictional drag in the system. Under such condition the velocity induced by active rotation does not drop to zero in bulk phase abruptly; rather it drops gradually from a maximum at the center of the interface to zero in the bulk phase within a flow region (Figure B.3). The characteristic length scale of this flow region in bulk can be determined by solving for the velocity profile in the bulk phase. There is no momentum source in bulk region; thus the dominant two terms in (B.22) are –

$$0 = \eta \frac{\partial^2 v_x}{\partial y^2} - b v_x \tag{B.29}$$

In dimensionless form –

$$0 = \eta \frac{Mr^{3/2} / K^{1/2}}{K / r} \frac{\partial^2 \tilde{v}_x}{\partial \tilde{y}^2} - b \frac{Mr^{3/2}}{K^{1/2}} \tilde{v}_x \tag{B.30}$$

$$\Rightarrow 0 = \frac{\partial^2 \tilde{v}_x}{\partial \tilde{y}^2} - \beta \tilde{v}_x \tag{B.31}$$

(B.31) is a homogeneous second order differential equation with characteristic equation –

$$\Omega^2 - \beta = 0 \Rightarrow \Omega = \pm \beta^{1/2} \tag{B.32}$$

The homogenous solution of (B.31) is given by

$$v_x = (c_0 + c_1) \exp(-\beta^{1/2} y) \tag{B.33}$$

Where c_0 and c_1 are constants. The velocity profile is described by (B.33) and the characteristic length scale of the flow region is given by $\beta^{-1/2}$. Since viscous damping is more dominant compared to the frictional damping the third term in (B.22) may be neglected for interfacial region –

$$\eta \frac{\partial^2 v_x}{\partial y^2} \sim \tau \frac{\partial \varphi}{\partial y} \tag{B.34}$$

Integrating with respect to *y* yields –

$$\int_0^{\delta} \left(\eta \frac{\partial^2 v_x}{\partial y^2} \sim \tau \frac{\partial \varphi}{\partial y} \right) dy \tag{B.35}$$

$$\Rightarrow \eta\left(\frac{\partial v_x}{\partial y}\right)_0^{\delta} \sim \tau(\varphi(\delta)-\varphi(0)) \tag{B.36}$$

Here it is assumed that the interface is symmetric about y = 0 and $\delta \sim (K/r)^{1/2}$ is the characteristic thickness of the interfacial region. Thus the boundary conditions become-

$$\varphi(0)=0 \text{ and } \left(\frac{\partial v_x}{\partial y}\right)_0 = 0 \tag{B.37}$$

Furthermore, $\varphi(\delta) \sim (r/\lambda)^{1/2}$ such that, (B.36) simplifies to

$$\eta\left(\frac{\partial v_x}{\partial y}\right)_{\delta} \sim \tau(r/\lambda)^{1/2} \tag{B.38}$$

Now assuming continuous velocity and velocity gradient between the interface and the bulk phases, it can be written-

$$v_x^{\text{int}erface}(\delta) = v_x^{bulk}(\delta) \tag{B.39}$$

and,

$$\left(\frac{\partial v_x^{\text{int}erface}}{\partial y}\right)_{\delta} = \left(\frac{\partial v_x^{bulk}}{\partial y}\right)_{\delta} \tag{B.40}$$

Combining (B.38) and (B.40) –

$$\eta\left(\frac{\partial v_x^{bulk}}{\partial y}\right)_{\delta} \sim \tau \tag{B.41}$$

Now using the solution of velocity profile in the bulk region, the velocity gradient can be approximated as –

$$\frac{\eta M r^2}{K}\frac{\tilde{v}_x}{\Delta\tilde{y}} \sim \tau (r/\lambda)^{1/2} \tag{B.42}$$

$$\Rightarrow U \sim \frac{\tau K (r/\lambda)^{1/2}}{\eta M r^2 \beta^{1/2}} \sim \frac{\alpha}{\beta^{1/2}} \tag{B.43}$$

Here U is the characteristic length scale in weak damping regime. Since the frictional damping is weak compared to the viscous damping, the dominant balance equation for this regime can be written from (B.22) as –

$$b v_x \ll \eta \frac{v_x}{(\Delta y)^2} \tag{B.44}$$

In dimensionless form –

$$b \ll \frac{\eta r}{K(\Delta\tilde{y})^2} \tag{B.45}$$

As $\Delta\tilde{y} \sim 1$ in the interfacial region thus (B.45) reduces to

$$\Rightarrow \beta \ll 1 \tag{B.46}$$

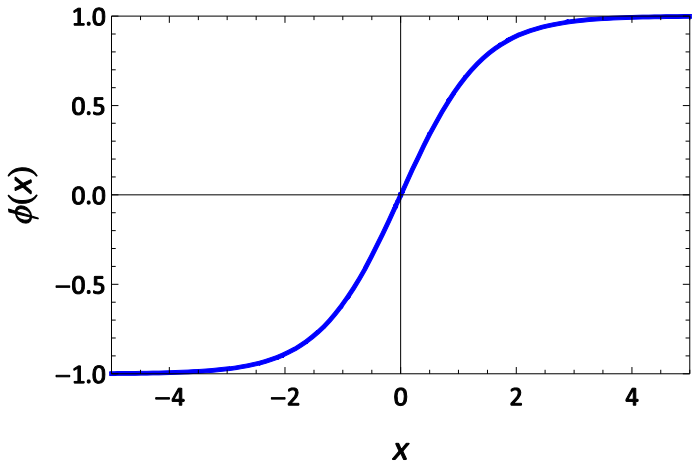

Figure B.1 1-dimensional solution of order parameter at long time ($t > 1$) in the bulk phase for flat equilibrium interface.

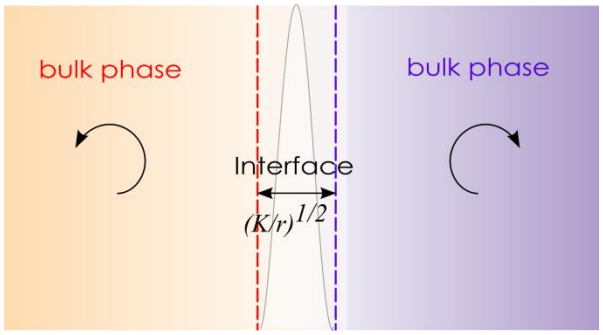

Figure B.2 Schematic flow profile in strong damping regime ($\beta \gg 1$). The gray line shows the expected velocity profile in the interfacial region. Flow due to the active rotation is confined within the interface only due to the strong frictional damping. The characteristic length scale for the interfacial region is shown in dimensional form.

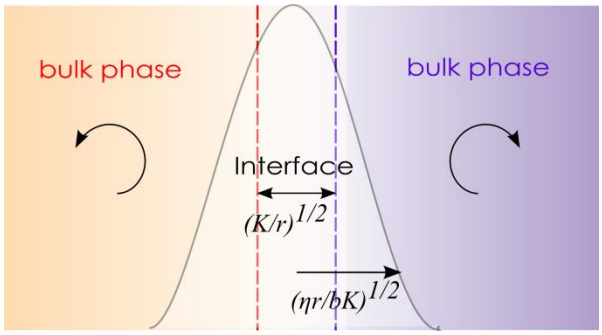

Figure B.3 Schematic flow profile in weak damping regime ($\beta \ll 1$). The gray line shows the expected velocity profile that extends into the bulk region in weak damping regime. The characteristic length scales for the interfacial region and the flow region are shown in dimensional form.